Chromium Sandwich Complexes of Polycyclic Aromatic Hydrocarbons: Triphenylene and Fluoranthene as η^6 Ligands

Christoph Elschenbroich*[1], Reinhart Möckel[A1], Alexander Vasil'kov[A2], Bernhard Metz[A1], and Klaus Harms[A1],

Fachbereich Chemie der Philipps-Universität Marburg[a],
Hans-Meerwein-Strasse, D-35032 Marburg, Germany
Fax: (internat.) + 49(0)6421/28-8917
E-mail: eb@ps1515.chemie.uni-marburg.de

A. N. Nesmeyanov Institute of Organoelement Compounds, Russian Academy of Sciences[b],
V-334 Vavilov st. 28, 117813 Moscow, Russia

Received March 10, 1998

Keywords: Polycycles / Sandwich complexes / Site preference / Cyclic voltammetry / NMR and EPR spectroscopy

The sandwich complexes bis(η^6-triphenylene)chromium (**12**) and bis(η^6-fluoranthene)chromium (**13**) have been prepared by means of metal atom/ligand vapor cocondensation. Whereas for triphenylene exclusive coordination to the peripheral rings is observed, the situation is more complicated for fluoranthene. According to NMR evidence initial metal coordination to the benzene (B) as well as to the naphthalene (N) section of the fluoranthene ligand occurs, leading to the isomers **13**(I) (η^6-B, η^6-B), **13**(II) (η^6-B, η^6-N) and **13**(III) (η^6-N, η^6-N). Since the substitutional lability of the chromium–naphthalene bond largely exceeds that of the chromium–benzene bond, the isomer distribution depends on the workup conditions; **13**(I) is clearly the most stable isomer. Crystal structure determinations performed for the salts [**12**][BPh_4] and [**13**][I] point to the preference for *syn* orientation of the polycyclic aromatic hydrocarbons and to a minute metal slippage in the peripheral direction. The triphenylene complex **12** features the electrochemically reversible redox couples **12** (+/0, metal-centered), **12** (0/–, ligand-centered) and **12** (–/2–, ligand-centered), the latter displaying a redox splitting of 300 mV. Conversely, for the fluoranthene complex **13**, secondary reduction **13** (–/2–) is irreversible. This finding is consistent with the larger redox splitting of ca. 480 mV which indicates more extensive interligand interaction in the dianion $\mathbf{13}^{2-}$, thereby favoring metal–ligand cleavage. While the radical cations $\mathbf{12}^{+\cdot}$ and $\mathbf{13}^{+\cdot}$ are amenable to EPR study, the radical anions $\mathbf{12}^{-\cdot}$ and $\mathbf{13}^{-\cdot}$ are too unstable. Instead, the radical anions of the free ligands are observed by EPR upon electrochemical reduction. In the case of **12**, the temporary existence of the radical anion $\mathbf{12}^{-\cdot}$ is indicated, however.

Introduction

Polycyclic aromatic hydrocarbons (PAHs)[2] have played an important role as potential ligands in sandwich complexes from the onset of bis(arene)metal chemistry. Fundamental questions deal with regioselectivity of coordination and the possibility of preparing oligonuclear complexes or even polymers with novel properties. PAHs as π ligands are encountered in a large number of carbonylmetal derivatives $[(PAH)metal(CO)_m]^{n+}$, in $[(PAH)metal(cyclopentadienyl)]^{n+}$ cations, in $[(PAH)metal(olefin)_m]^{n+}$ cations and in a few complexes of the type [(PAH)metal(phosphane)$_n$][3]. Conversely, the number of sandwich complexes (η^6-PAH)$_2$metal is very limited, the species $\mathbf{1}^{2-}$[4], **2**[5a], **3**[5], **4**[6], $\mathbf{5}^{2+}$[7], **6**[8], $\mathbf{7}^{+}$[9], **8**[10] being the only examples characterized to date. The dianion $[(C_{10}H_8)_3Zr]^{2-}$ features bent naphthalene ligands and η^4 coordination[11]. The synthesis of binary complexes of transition metals and polycyclic hydrocarbons is desirable since it is only in the absence of auxiliary ligands that the basic questions addressed below may be studied unequivocally.

An ubiquitous feature of the coordination chemistry of polycyclic aromatic hydrocarbons is the ease of ligand hydrogenation during the course of wet chemical synthesis. Thus, early attempts to prepare bis(naphthalene)chromium by means of the Fischer−Hafner synthesis afforded bis(tetralene)chromium and the Nesmeyanov reaction was frequently accompanied by partial hydrogenation of the PAH. Therefore, metal atom/ligand vapor cocondensation techniques were originally used. Recently, the reaction of conventionally generated alkali metal naphthalenides with $MCl_3(THF)_3$ (M = V, Cr, Mo) and $MoCl_4(THF)_2$ has been introduced as a convenient method for the synthesis of bis(η^6-naphthalene)metal complexes[12]. Here we report on the binary chromium complexes of triphenylene **9** and fluoranthene **10**. These ligands are examples of the two types of condensation, triphenylene (**9**) representing the *kata* and fluoranthene (**10**) the *peri* principle. Furthermore, **9** is an alternant and **10** a nonalternant PAH. **9** and **10** may also be regarded as benzene rings with a biphenyl or a naphthalene unit, respectively, fused to them.

Fundamental questions in PAH coordination chemistry relate to site selectivity of bonding and to the possibility of

[◇] Part 51: Ref.[1].

  1434−1948/98/1010−1391 $ 17.50+.50/0

Scheme 1

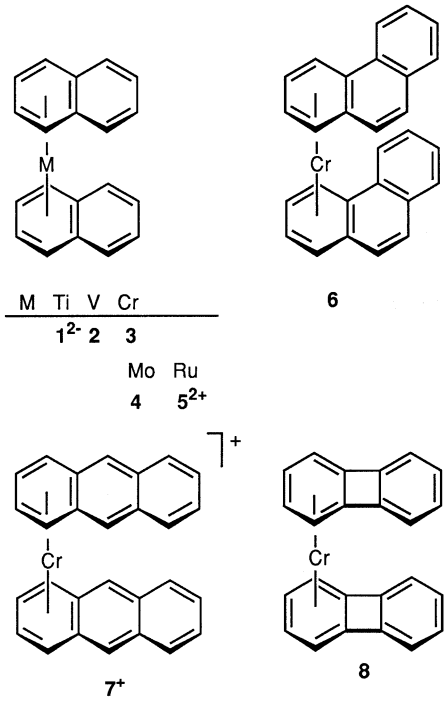

Scheme 2

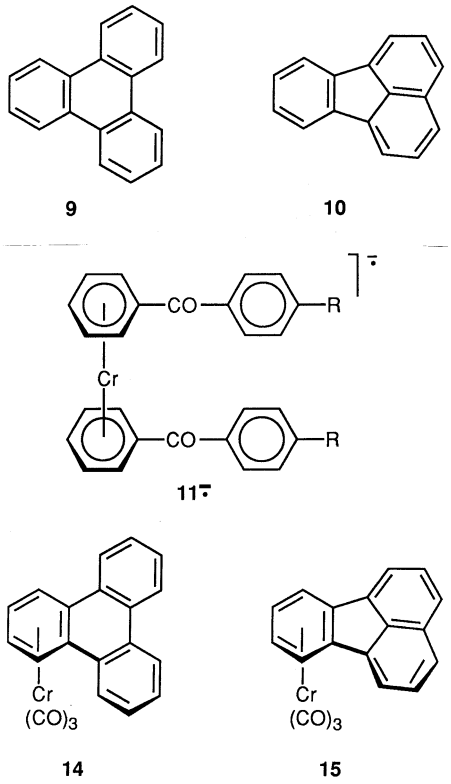

haptotropic shifts. Furthermore, in the case that in their η^6-coordinated state the ligands **9** and **10** maintain their ability to accept an additional electron forming radical anions, the question as to the rate of intramolecular electron transfer (ET) arises, since spin localization in one ligand as well as rapid interligand ET (delocalization) is conceivable. This dichotomy has previously been studied using EPR for benzoyl derivatives of bis(benzene)chromium ($\mathbf{11}^{-\cdot}$)[13]. Finally, interligand communication should also be apparent from an eventual redox splitting $\delta E_{1/2}$ exhibited by primary and secondary reduction of the complexes (η^6-PAH)$_2$Cr.

Results and Discussion

As has been demonstrated in the past for PAHs, metal atom/ligand vapor cocondensation techniques (CC) circumvent the problem of ligand hydrogenation and we therefore applied this method to the synthesis of bis(η^6-triphenylene)chromium (**12**) and bis(η^6-fluoranthene)chromium (**13**) (Scheme 3). The new complexes **12** and **13** were obtained in low yield as, respectively, brown or dark-violet air-sensitive solids which were only sparingly soluble in common organic solvents. The isomers **13**(II) and **13**(III) will be dealt with later. The separation of excess ligand from metal complex is a common problem in the metal-vapor technique of synthesis; it is particularly aggravating in the case of PAHs since the solubilities of the ligands and of the neutral complexes are often very similar. Conversion of the complex to its radical cation and extraction with water is not generally applicable since certain complex cations (η^6-PAH)$_2$Cr$^+$ are labile with respect to solvolysis (example: PAH = naphthalene[5]). However, the radical cations $\mathbf{12}^{+\cdot}$ and $\mathbf{13}^{+\cdot}$ are moderately inert in aqueous solution if kept in the dark; the photolability of $\mathbf{13}^{+\cdot}$ clearly exceeds that of $\mathbf{12}^{+\cdot}$. Thus, the redox cycle [**12** (**13**) $-$ e$^-$ $\rightarrow$ $\mathbf{12}^{+\cdot}$ ($\mathbf{13}^{+\cdot}$); extraction; $\mathbf{12}^{+\cdot}$ ($\mathbf{13}^{+\cdot}$) + e$^-$ $\rightarrow$ **12** (**13**)] can be utilized to effect separation of the complex from excess free ligand.

Single crystals suitable for X-ray diffraction could only be obtained for the complex cations $\mathbf{12}^{+\cdot}$ and $\mathbf{13}^{+\cdot}$ with BPh_4^- or I$^-$ serving as the counterion. Views of the structures are presented in Figures 1 and 2; bond lengths and bond angles are collected in the captions. Structural discussions of the class of compounds treated here should address the conformation in the solid state, ring slippage and the modification of ligand geometry induced by metal coordination. In **12**, as well as in **13**, chromium coordinates to the ring with the highest index of local aromaticity (ILA)[14] i.e. the ring which among the canonical forms most frequently appears with a Kekulé structure; this is a peripheral ring in **12** and the benzene (rather than the naphthalene) unit in **13**. The same site preference is adopted by the Cr(CO)$_3$ fragments in **14**[15] and **15**[16]. The complex cation in [**12**][BPh_4] adopts a conformation with regard to the sandwich axis which may be designated as synclinal, the torsional angle being 23.6°. This differs from the exact synperiplanar conformation which prevails in the related neutral complexes **3**[5b] and **8**[10]. Conceivably, the twisted disposition of the two ligands in $\mathbf{12}^+$, which is reminiscent of the graphite lattice, reduces interannular π-electron repulsion and is favored by the less dense packing in the complex salt [**12**][BPh_4] compared to the neutral complexes **3** and **8**.

For the salt [**13**][I], which contains the less bulky counterion I$^-$, the conformation with regard to the sandwich axis is synperiplanar. Interestingly, incorporation of solvent

Scheme 3

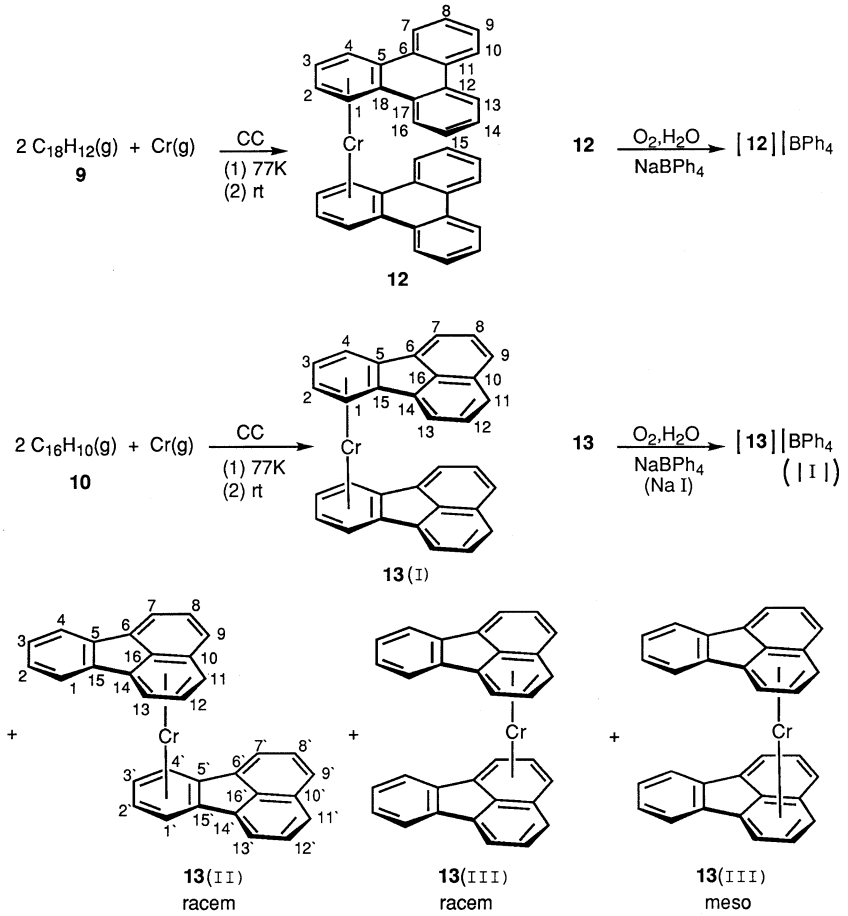

molecules in the lattice, as well as the use of a larger counterion, causes deviations of the conformation of $\mathbf{13}^{+\cdot}$ from exact synperiplanarity; for specimens of [**13**][I]·0.5 acetone and [**13**][BPh_4] torsional angles of 6.7° and 16.5° respectively were determined using X-ray diffraction[17]. Obviously, for sandwich complexes of PAHs packing forces are an important factor in the establishment of a certain ligand−metal−ligand disposition, probably overriding electronic factors. Ring slippage is minute in the structures of the cations $\mathbf{12}^{+\cdot}$ and $\mathbf{13}^{+\cdot}$; it is directed toward the ligand periphery and amounts to 3.9 pm ($\mathbf{12}^{+\cdot}$) and 5.2 pm ($\mathbf{13}^{+\cdot}$). A similar slippage has been reported for the half-sandwich complex (η^6-triphenylene)$Cr(CO)_3$[15]. Ring tilting is small as well, in that the deviations of the PAH ligands from a parallel disposition amount to 3.5° only for $\mathbf{12}^{+}$ and $\mathbf{13}^{+}$, the larger interplanar distance being encountered in the noncoordinated region; η^6 coordination renders the three peripheral rings of triphenylene structurally inequivalent in that the metal-bonded ring features significantly enlarged C−C bond lengths. Although the weighted average bond length of the free peripheral C rings amounts to 139 pm, that of the η^6-arene is 141 pm. The average C−C bond length for the central ring, which contributes two carbon centers to the coordinate bond, is 144 pm. This value exceeds the respective number for the free ligand triphenylene[18] by 1 pm and reflects the usual finding that in bis(arene)metal coordination δ backbonding M-δ→L is slightly more effective than σ, π donation M←σ,π-L. Bond length alternation in the central ring reflects the existence of three largely independent 6-π-electron systems in the peripheral rings and is, of course, also observed for the complex cation $\mathbf{12}^{+\cdot}$.

A similar trend is exhibited by the C−C bond lengths in (η^6-fluoranthene)$_2Cr^{+\cdot}$ ($\mathbf{13}^{+\cdot}$); the geometry of the naphthalene moiety is identical to that in the free ligand fluoranthene[19] while the η^6-benzene unit shows the typical increase of 2 pm for the C−C distances. The bonds C(5)−C(6), C(5′)−C(6′) and C(14)−C(15), C(14′)−C(15′) which connect the benzene and naphthalene moieties possess a mean length of 147 pm; thus, in the complex **13**, as well as in the free ligand **10**, naphthalene is linked to benzene by single bonds.

The site of chromium coordination in **12** and **13** follows, inter alia, from the ^{1}H-NMR spectra which in the case of the triphenylene complex **12** unambiguously demonstrate η^6 bonding to a peripheral ring. The relevant data are found

Figure 1. Molecular structure of compound [**12**][BPh_4]; top: SHELXTL/XP drawing with 50% probability ellipsoids; bottom: SHELXTL/XP drawing showing the ligand−metal−ligand torsion; C−*H* atoms omitted for clarity[a]

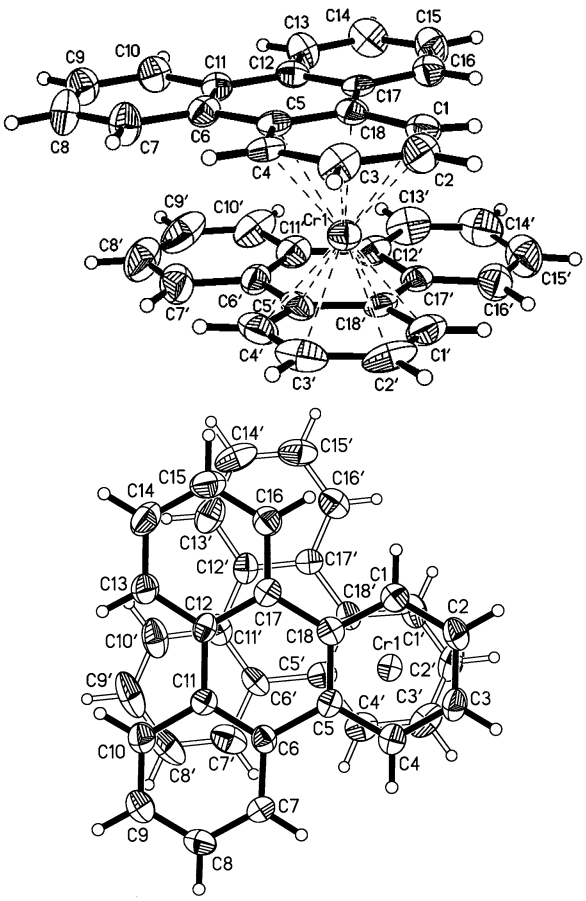

[a] Selected bond lengths [Å]: C1−C2 1.402(6), C2−C3 1.394(6), C3−C4 1.408(7), C4−C5 1.423(6), C5−C18 1.427(6), C1−C18 1.426(7), C5−C6 1.478(6), C6−C7 1.397(6), C7−C8 1.373(7), C8−C9 1.381(6), C9−C10 1.366(6), C10−C11 1.413(7), C11−C12 1.470(6), C12−C17 1.417(6), C12−C13 1.402(6), C13−C14 1.369(6), C14−C15 1.388(7), C15−C16 1.364(6), C16−C17 1.400(6), C17−C18 1.464(6), Cr1−C1 2.145(5), Cr1−C2 2.147(4), Cr1−C3 2.140(5), Cr1−C4 2.135(5), Cr1−C5 2.182(6), Cr1−C18 2.227(5); interplanar angle [°]: tilt of best ligand planes 3.50(7); torsional angle [°]: C1−C2−C2′−C1′ 23.6; ring slippage [Å]: (Cr displacement toward ligand periphery) 0.037(2).

in Table 1. The spectrum initially obtained is unaffected by heating, therefore isomerization by haptotropic metal shifts is absent. Assignment of the chemical shifts δH(1, 4) and δH(2, 3) is based on their coordination shifts and on linewidth considerations; unresolved inter-ring coupling broadens the multiplet at lower field compared to that at higher field. Differentiation between δH(7, 16) and δH(10, 13) is achieved by means of selective homonuclear decoupling in that irradiation at δH(7) = 7.4 sharpens the signal δH(1, 4); differentiation between δH(8, 15) and δH(9, 14) follows from the effect of irradiation at δH(10) = 7.78 on the former two multiplets. It may be noted that apart from the usual, large coordination shifts Δδ*H* = −3.1 experienced by the protons H(1−4) which are directly bonded to an η-C atom, the protons H(7−10, 13−16) on the noncoordinated rings in **12** also display considerable upfield shifts.

Figure 2. Molecular structure of compound [**13**][I], SHELXTL/XP drawing viewed perpendicular and parallel to the sandwich axis; C−*H* atoms omitted for clarity[a]

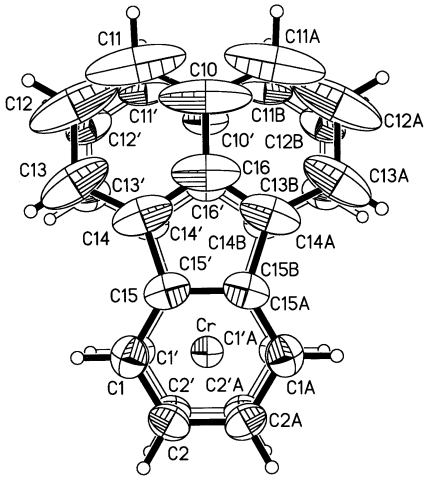

[a] Selected bond lengths [Å]: C1−C2 1.401(5), C2−C2A 1.407(7), C1−C15 1.393(5), C15−C15A 1.457(7), Cr−C1 2.149(3), Cr−C2 2.135(4), Cr−C2A 2.135(4), Cr−C1A 2.149(3), Cr−C15A 2.179(3), Cr−C15 2.179(3); interplanar angle [Å]: tilt of best ligand planes 3.70(8); torsional angle C1−C2−C1′−C2′ 0.2°; ring slippage [Å]: (Cr displacement toward ligand periphery) 0.036(6).

This probably reflects the temporary existence in solution of rotamers, which place one ligand in the shielding region (ring current) of the other. ^{13}C NMR of **12** suffers from low solubility; this calls for broad-band proton decoupling. A compilation of the chemical shifts and their provisional analysis is also given in Table 1. Whereas the differentiation between metal-coordinated and free positions is trivial in view of the large coordination shifts of the former, specific assignments are less secure. They are based on intensity criteria and on comparisons with the related complexes bis(naphthalene)chromium (**3**)[5c], bis(fluorene)chromium[20], and bis(9,10-dihydroanthracene)chromium[9] for which unequivocal analysis has been possible.

While NMR study of the *triphenylene* complex **12** was straightforward, essentially confirming the structural characteristics gleaned from X-ray diffraction, more complicated, albeit informative, NMR behavior is exhibited by the *fluoranthene* complex **13**. The complications arise from isomerism for which the spectra provide evidence; the additional information concerns the occurrence of haptotropic shifts which explain the spectral changes effected by modifying the workup conditions and upon thermal treatment of solutions of neutral **13**. As shown in Scheme 3, complex **13** may exist as an achiral bis(η^6-benzene) form (I), a pair of enantiomers featuring (η^6-benzene)(η^6-naphthalene) coordination (II) and a bis(η^6-naphthalene) variant (III) which should generate a pair of enantiomers and a *meso* form. Experimental evidence,[2][3][4] as well as local aromaticity (ILA) considerations,[14] suggest that coordination to a benzene ring is favored over bonding to a naphthalene unit, rendering isomer I the thermodynamically most stable product. Therefore, if the purification process, which consists of separating the water-soluble cation $\mathbf{13}^+$ from excess ligand is carried out at leisure, i.e. exposing $\mathbf{13}^+$

to the aqueous medium for one hour or more, the isomers featuring the labile (η^6-naphthalene) coordination are solvolytically cleaved and pure **13**(I) is isolated after reduction. The ^{1}H-NMR pattern in the η^6-arene region is depicted in Figure 3a; spectral parameters are collected in Table 2. Thermal treatment of this probe does not cause spectral changes, thereby confirming that in fact, **13**(I) is the most stable isomer.

Table 1. ^{1}H- and ^{13}C-NMR data for the ligand **9** and the complex **12**

Position	**9**[a]	**12**[a]	Δδ(**9**, **12**)[a]	**9**[b]	**12**[b]	Δδ(**9**, **12**)[b]
1, 4	8.42	5.39	−3.03	123.71	72.40	−51.31
2, 3	7.39	4.44	−2.95	127.38	78.23	−49.15
5, 18				130.35	84.41	−45.94
6, 17				130.35	135.02	+4.67
7, 16	8.42	7.40	−1.02	123.71	122.87	−0.84
8, 15	7.39	7.00	−0.39	127.38	125.26	−2.12
9, 14	7.39	7.19	−0.20	127.38	126.51	−0.87
10, 13	8.42	7.78	−0.64	123.71	123.22	−0.49
11, 12				130.35	130.11	−0.24

[a] δ^1H in C_6D_6 − [b] δ^{13}C in C_6D_6; coupling constants $J(^1H,^1H)$ [Hz]: **9**: *J*(1,2; 3,4; 7,8; 10,9; 13,14; 15,16) = 8.4, *J*(1,3; 2,4; 7,9; 8,10; 13,15; 14,16) = 1.3, *J*(1,4; 7,10; 13,16) = 0.5, *J*(2,3; 8,9; 14,15) = 6.8. − **12**: *J*(1,2; 3,4) = 5.5, *J*(1,3; 2,4) = 0.7, *J*(2,3) = 5.2, *J*(7,8; 15,16) = 7.5, *J*(7,9; 14,16) = 1.3, *J*(8,9; 14,15) = 7.3, *J*(8,10; 13,15) = 1.2, *J*(9,10; 13,14) = 7.9.

Table 2. ^{1}H-NMR data for the ligand **10**, the isomeric complexes **13**(I), **13**(II), **13**(III), and the complex **16**

Position	**10**[a]	**13**(I)[a]	**13**(II)[a]	**13**(III)[a]	**16**[a]
1 (1, 1′)[b]	7.73	4.86	(7.63, 5.13)	8.08	5.49
2 (2, 2′)	7.24	4.45	(7.34, 4.75)	7.40	4.67
3 (3, 3′)	7.24	4.45	(7.24, 4.52)	7.54	4.67
4 (4, 4′)	7.73	4.86	(7.55, 4.71)	8.03	5.49
7 (7, 7′)	7.64	6.83	(7.03, 6.75)	5.34	
8 (8, 8′)	7.37	7.08	(6.64, 7.20)	4.79	
9 (9, 9′)	7.61	7.35	(7.06, 7.44)	5.86	
11 (11, 11′)	7.61	7.35	(5.42, 7.42)	7.98	
12 (12, 12′)	7.37	7.08	(4.61, 7.37)	7.52	
13 (13, 13′)	7.64	6.83	(4.99, 7.05)	7.81	
17					3.76[c]

[a] δ^1H in C_6D_6; for the numbering see Scheme 3. − [b] In **13**(II). − [c] ^{2}H NMR in C_6H_6; coupling constants $J(^1H,^1H)$ [Hz]: **10**: *J*(7,8; 12,13) = 6.9, *J*(7,9; 11,13) = 0.5, *J*(8,9; 11,12) = 8.2, *J*(1,2; 3,4) = 7.6, *J*(1,3; 2,4) = 1.0, *J*(1; 4) = 0.7, *J*(2,3) = 7.5. − **13**(I): *J*(7,8; 12,13) = 6.9, *J*(7,9; 11,13) = 0.5, *J*(8,9; 11,12) = 8.2, *J*(1,2; 3,4) = 5.3, *J*(1,3; 2,4) = 0.7, *J*(1,4) = 0.8, *J*(2,3) = 5.2. − **13**(II): *J*(1′,2′; 3′,4′) = 5.5, *J*(2′,3′) = 5.2, *J*(11,12) = 5.3, *J*(12,13) = 5.5. − **13**(III): *J*(7,8) = 5.4, *J*(8,9) = 5.2. − **16**: *J*(1,2; 3,4) = 5.3, *J*(1,3; 2,4) = 0.6, *J*(1,4) = 0.6, *J*(3,2) = 5.0.

With the aim of identifying the less stable isomers, the redox procedure which effects the separation of unreacted excess ligand which is soluble in benzene from the water-soluble complex cation $\mathbf{13}^{+\cdot}$ was performed expeditiously, such that the mixture of primary cocondensation products was exposed to the aqueous medium for less than 10 minutes. After reduction to the neutral complex stage, ^{1}H NMR indicated the presence of two species A and B in a ratio of ca. 1:6. Attempts to isolate in pure form the species giving rise to spectrum B failed; however, after repeated crystallization of the product mixture, species B could be enriched to a composition A/B = 1:20 (Figure 3b). The ^{1}H-NMR spectrum of this sample was unchanged up to 80°C, whilst heating to 100°C led to the gradual disappearance of spectrum B and to the emergence of two new spectra C and D. During prolonged heating, spectrum D grew at the expense of spectrum C (Figures 3c−e). During all these manipulations the intensity of A remained approximately constant.

Table 3. ^{13}C-NMR data for the ligand **10**, the isomeric complexes **13**(I), **13**(II), **13**(III), and the complex **16**

Position	**10**[a]	**13**(I)[a]	**13**(II)[a]	**13**(III)[a]	**16**[a]
1 (1, 1′)[b]	121.91	76.27	(120.48, 77.05)	122.07	72.88
2 (2, 2′)	127.81	78.58	(127.66, 77.23)	124.58	74.26
3 (3, 3′)	127.81	78.58	(124.24, 76.48)	126.24	74.26
4 (4, 4′)	121.91	76.27	(121.74, 78.01)	120.79	72.88
7 (7, 7′)	120.35	117.19	(118.04, 117.59)	73.56	
8 (8, 8′)	128.22	128.00	(128.11, 128.29)	78.01	
9 (9, 9′)	126.89	123.14	(132.89, 123.08)	73.38	
11 (11, 11′)	126.89	123.14	(76.88, 123.04)	134.98	
12 (12, 12′)	128.22	128.00	(81.82, 127.91)	128.30	
13 (13, 13′)	120.35	117.19	(76.70, 117.47)	115.35	
17					80.29[c]

[a] δ^{13}C in C_6D_6; for the numbering see Scheme 3. − [b] In **13**(II). − [c] Triplet.

In order to interpret this evolution we start from the premise that the metal−ligand cocondensation process initially yields a mixture of isomers stemming from statistical, unspecific coordination of chromium atoms to all of the available benzenoid moieties. Extended exposure to an aqueous medium will lead to solvolytic cleavage of all of those species which contain either one or both sandwich ligands in an η^6-naphthalene coordination mode. Therefore, only **13**(I) survives in which both fluoranthene ligands bind to chromium via their benzene section. It is well known that in bis(naphthalene)chromium (**3**) the "first" naphthalene ligand is substitutionally more labile than the "second"[6a]. Thus, spectrum B, which is detected in addition to A after fast workup, should belong to isomer **13**(II). This suggestion is borne out by the observation of seven inequivalent proton signals, four doublets and three triplets, in the shift range characteristic for η-arene protons. The assignment given in Table 2 is based on HH-COESY and NOESY experiments. Spectrum C which dominates after thermal treatment points to isomer **13**(III) in which both ligands engage in coordination to chromium via a benzenoid system belonging to the naphthalene section. Apparently **13**(II) and **13**(III) exist in thermal equilibrium, the less stable isomer **13**(III) being formed at higher temperature, albeit at a small rate of interconversion. The room-temperature spectrum Figure 3d may therefore reflect a metastable state. Spectrum D which is also visible at this stage shows a simple AA′XX′ pattern, thereby indicating the presence of only *one* coordination mode, namely η^6 bonding via the benzene moiety. Since the chemical shifts in spectrum D differ from those observed for **13**(I) it must be assumed that

Figure 3. ^{1}H-NMR spectra (η^6-arene shift range, C_6D_6, room temperature) of the products from cocondensing fluoranthene vapor with chromium atoms; (a) after workup with extended (90 min) exposure to an aqueous medium; (b) after workup with short ($\leq$ 10 min) exposure to an aqueous medium and repeated recrystallization to enrich component B (A/B $\approx$ 1:20); (c) after subjecting probe b to 100°C for 8d; (d) after 16 d at 100°C; (e) after 42 d at 100°C

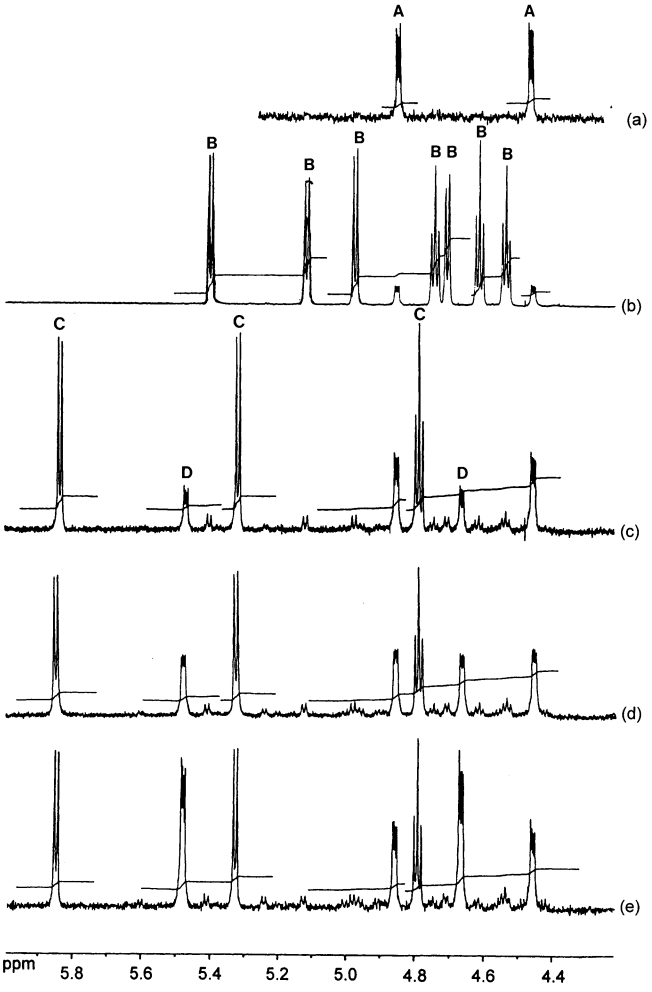

a second ^{1}H-NMR-silent ligand completes the coordination sphere. C_6D_6, the solvent molecule, could be a likely candidate, introduced by ligand substitution leading to (η^6-fluoranthene)(η^6-deuterobenzene)chromium (**16**). In order to test this hypothesis, thermal treatment of a mixture of **13**(I) and **13**(II), dissolved in C_6D_6, was repeated and at various time intervals, after having recorded the ^{1}H-NMR spectrum, the solvent C_6D_6 was removed in vacuo and replaced by C_6H_6. The solutions thus obtained were subjected to ^{2}H NMR. It was found that build-up of the ^{1}H-NMR spectrum C correlates with the observation in ^{2}H NMR of a singlet at δ = 3.76, the characteristic chemical shift for η^6-benzene. This attests to ligand substitution of fluoranthene by benzene. Based on the NMR observations, the course of events may therefore be sketched as shown in Scheme 4.

The redox behavior of the complexes **12** and **13**, not surprisingly, reflects the properties of the bis(η^6-arene)chromium core and those of the ligands triphenylene **9** and fluoranthene **10**. Cyclovoltammetric traces are depicted in Figures 4 and 5; the electrochemical parameters are given in

Scheme 4

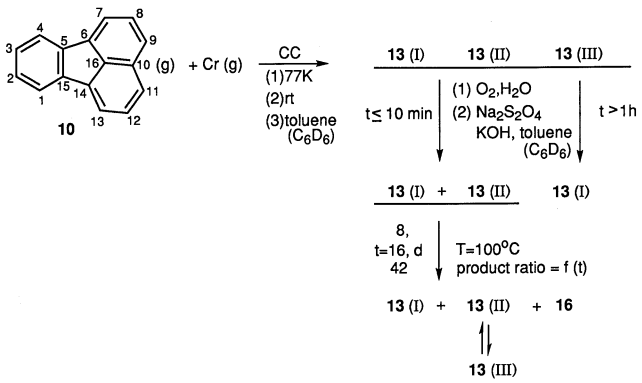

the captions. The redox couples $E_{1/2}$ (**12**$^{+/0}$) = −0.62 V and $E_{1/2}$ (**13**$^{+/0}$) = −0.64 V are reversible and deviations from the peak current ratio $p_c/p_a = 1$ are probably due to adsorption effects. The magnitudes of the potentials differ only marginally, which is plausible in view of the fact that the redox orbital is essentially metal centered[21]. Changes in the ligand periphery therefore exert only an indirect influence. Conversely, the reduction processes as gauged by the potentials $E_{1/2}$ (**12**$^{0/-}$), E(**12**$^{-/2-}$) and E(**13**$^{0/-}$), E(**13**$^{-/2-}$), respectively, mirror the differing electron affinities of triphenylene and fluoranthene, again in accord with the electronic structure of bis(arene)chromium which assigns considerable ligand participation to the LUMO. Thus, compared to **12**, electron transfer to **13** occurs at a somewhat more positive potential. This gradation also applies to the free ligands **10** and **9**[22]. Relative to the free ligands **9** and **10**, reduction of the complexes **12** and **13** features cathodic shifts; this accords with the ligand-dominated nature of the LUMO in bis(arene)metal complexes and the fact that the η^6-arenes bear a negative partial charge[21b]. For the triphenylene complex, a second reduction step can be observed which, as judged from the peak separation, appears to be reversible too. The peak current ratio is difficult to assess at this negative potential near the cathodic limit imposed by the medium. It is worth mentioning that the cyclovoltammogram of **12** does not feature waves which indicate the presence of free ligand. Therefore, bis(triphenylene)-chromium must be fairly robust, at least in the oxidation states **12**$^{+,0,-}$, although the potential separation δE(0/−, −/2−) = 300 mV between primary and secondary reduction demonstrates appreciable interligand interaction. For the fluoranthene complex **13** this interaction seems to be even more pronounced since δE(0/−, −/2−) = 480 mV is larger. Consequently, the second reduction step **13**$^{-/2-}$ is irreversible and the cyclovoltammogram contains weak waves which point to the presence of free fluoranthene, generated through metal−ligand bond cleavage. Therefore, strictly speaking, the value δE(**13**$^{0/-,\ -/2-}$) given above is only a rough estimate.

The differing robustness of **12** and **13** against solvolytic cleavage also emanates from the EPR spectra; these are depicted in Figures 6 and 7, with the EPR parameters listed

Figure 4. Cyclic voltammogram of complex **12** at −40°C in 1,2-dimethoxyethane/0.1 M tetrabutylammonium perchlorate: working electrode, glassy carbon; reference electrode, SCE; $v = 100$ mVs^{-1}. $E_{1/2}$(**12** +/0) = −0.62 V, ΔE_p = 44 mV, r = 0.7; $E_{1/2}$(**12** 0/−) = −2.31 V, ΔE_p = 90 mV, r = 1.0; $E_{1/2}$(**12** −/2−) = −2.61 V, $\Delta E_p \approx$ 80 mV, $r \approx 0.5$; E_{pa} = 0.85 V (irreversible secondary oxidation)

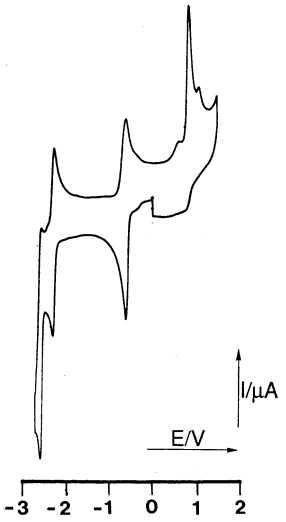

Figure 5. Cyclic voltammogram of complex **13** at −40°C in dimethoxyethane/0.1 M tetrabutylammonium perchlorate: working electrode, glassy carbon; reference electrode, SCE. $v = 100$ mVs^{-1}; $E_{1/2}$(**13** +/0) = −0.62 V, ΔE_p = 60 mV, r = 0.7; $E_{1/2}$(**13** 0/−) = −1.87 V, ΔE_p = 86 mV, $r \approx 1.1$ (cannot be measured accurately due to overlap with free ligand reduction); E_{pc} = −2.39 V (irreversible secondary reduction); E_{pa} = 0.65 (irreversible secondary oxidation); the shoulders marked L, are caused by first and second reduction of the free ligand **10**: $E_{1/2}$(**10** 0/−) = −1.73 V, ΔE_p = 54 mV, r = 0.76; E_{pc} = −2.21 V (irreversible secondary reduction); these data agree with those obtained from a control experiment with pure **10**

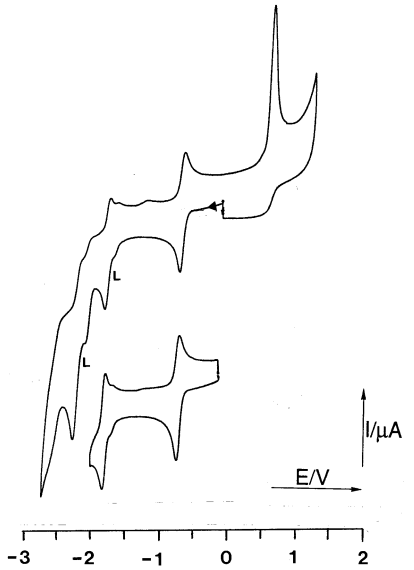

in the captions. The EPR spectra of the radical cations $\mathbf{12}^{+\cdot}$ and $\mathbf{13}^{+\cdot}$, generated either by air oxidation or electrochemically, differ in the extent to which chemically nonequivalent proton sites are resolved in the hyperfine structure. For $\mathbf{13}^{+\cdot}$ (Figure 7c) a pattern is observed which is consistent with eight equivalent protons, a(8 ^{1}H) = 0.34 mT, the difference between the coupling constants a(4 ^{1}H 1, 4) and a(4 ^{1}H 2, 3) not being resolved. Conversely, for $\mathbf{12}^{+\cdot}$ experiment and simulation yield the parameters a_1(4 ^{1}H) = 0.32 mT and a_2(4 ^{1}H) = 0.395 mT. Independent assignment of these coupling constants to positions at the ring cannot be made in the absence of specific deuteration. Thus, taking into consideration the aggregate nature of the mechanism of spin transfer from the central metal to ring protons in bis(arene)metal complexes[23], attempts to interpret in detail the 20% difference in the two experimental proton coupling constants for $\mathbf{12}^{+\cdot}$ would not be worthwhile. An aspect which should be addressed here, however, is the isomerism of the fluoranthene complex **13** which was discussed in the NMR section and which would be expected to manifest itself in the EPR spectra of the corresponding radical cations as well. As in the NMR study, we therefore varied the workup protocol in order to search for spectral differences. The results are depicted in Figure 7. A surprising observation is the detection of an EPR signal in the original cocondensation *before* oxidation to the radical cation (Figure 7a). While the basic features of this spectrum are characteristic of a bis(π-perimeter)chromium(d^5) species, the hyperfine pattern is unexpected since it shows coupling to *four* equivalent protons only. This can only be reconciled with a structure in which one of the fluoranthene ligands is η^6-bonded via its benzene moiety, the remainder of the coordination sphere being EPR silent. A possibility would be that the second fluoranthene ligand binds to chromium with the central, five-membered ring which is devoid of protons. Interestingly, the EPR parameters observed for this species [a(4 ^{1}H) = 4.38, a(^{53}Cr) = 15.4 G], apart from proton hyperfine multiplicity, differ significantly from the data typical for a bis(η^6-arene)Cr$^{+\cdot}$ radical cation such as $\mathbf{13}^{+\cdot}$ [a(8 ^{1}H) = 3.4, a(^{53}Cr) = 18.3 G]; they are very similar to the coupling constants reported for (η^5-C_5H_5)Cr(η^6-C_6H_6) [a(5 ^{1}H) = 2.35, a(6 ^{1}H) = 4.65, a(^{53}Cr) = 14.68 G[24]], however, thereby lending support to the proposal given above. On the other hand, coordination of chromium to the central five-membered ring is difficult to reconcile with the structural data of the ligand **9.** For this ligand the lengths of the bonds connecting the benzene and the naphthalene moieties are close to those of single bonds[18]. Furthermore, the presence of Cr(d^5), formally Cr^{1+}, would require a negatively charged ligand in the species under consideration, assuming that the latter is neutral. While in the parent complex (η^6-C_6H_6)Cr^{I}(η^5-C_5H_5) the negative charge of the cyclopentadienyl ligand results from deprotonation of C_5H_6, in the case of the primary radical complex in the cocondensation of chromium atoms with fluoranthene metal→ligand single-electron transfer could lead to an anionic ligand. This would, however, generate a biradical for which EPR fails to provide evidence. The nature of the species giving rise to the primary EPR signal cannot, therefore, be determined definitively.

In the NMR study, the critical factor leading to differences in the product distribution was the duration of exposure to an aqueous medium during the workup process.

Figure 6. EPR spectra of (a) the radical cation $\mathbf{12}^{+\cdot}$, (b) the radical anion $\mathbf{12}^{-\cdot}$ and (c) the radical anion $\mathbf{9}^{-\cdot}$ of the free ligand, generated electrochemically in situ (gold cathode, DME, nBu$_4$NPF$_6$, −40°C); the applied potential was gradually increased to 5 V; (d): $\mathbf{12}^{+\cdot}$ in CH_3OH at −30°C, second derivative trace and simulation; $\mathbf{12}^{+\cdot}$: $\langle g\rangle = 1.986$, $a_1(4\ ^1H) = 3.2$ G, $a_2(4\ ^1H) = 3.95$ G, $a(^{53}Cr) = 18.22$ G; $\mathbf{12}^{-\cdot}$: $\langle g\rangle = 1.991$, hyperfine pattern irregularly spaced; $\mathbf{9}^{-\cdot}$: $\langle g\rangle = 2.0037$; 1 G = 0.1 mT

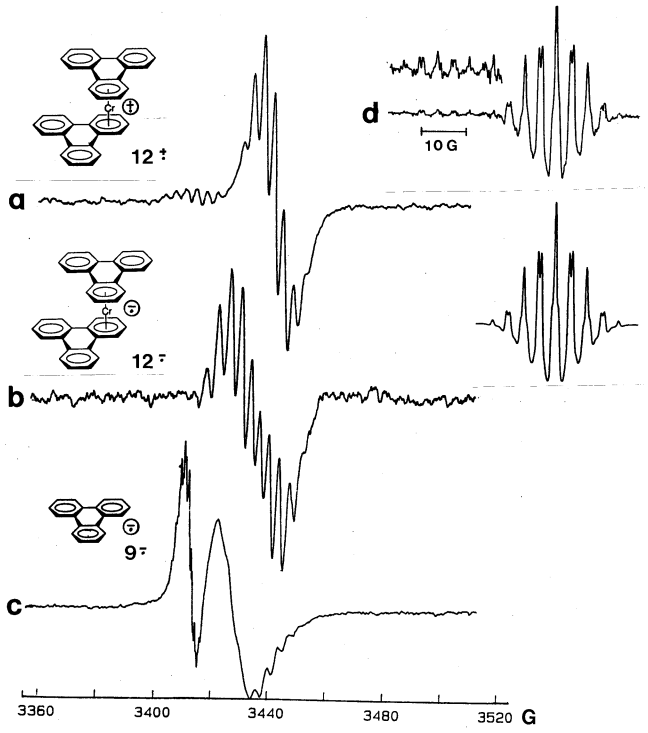

Figure 7. EPR spectra of products from the cocondensation of fluoranthene **10** with chromium atoms; (a) initial product mixture extracted with toluene, exclusion of oxygen $\langle g\rangle = 1.9892$, $a(4\ ^1H) = 4.38$ G, $a(^{53}Cr) = 15.4$ G, lower trace simulated; (b) spectrum observed after short exposure of the cocondensate to oxygen, reduction and reoxidation in an aprotic medium (DME), $\langle g\rangle = 1.9888$, $a(7\ ^1H) = 3.43$ G, $a(^{53}Cr) = 18.13$ G; (c) spectrum observed upon extraction of cocondensate with CH_3OH, access of oxygen, for 1 h, −40°C, $\langle g\rangle = 1.9871$, $a(8\ ^1H) = 3.40$ G, $a(^{53}Cr) = 18.3$ G; (d) spectral change caused by electrochemical intra muros reduction of probe b, applied potential −3.8 V; the well-resolved spectrum at low field belongs to the free ligand radical anion $\mathbf{10}^{-\cdot}$.

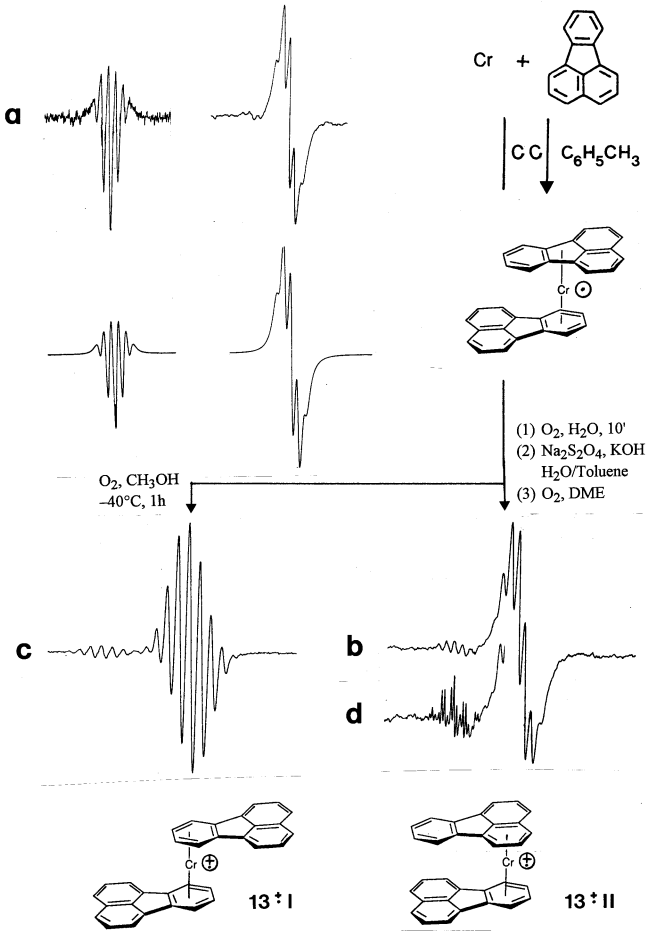

This parameter also governs the nature of the EPR spectra obtained. The fast workup variant led to a sample which gave rise to the ^{1}H-NMR spectrum shown in Figure 3b, which was assigned to isomer **13**(II). When this sample was oxidized in DME as a solvent to its radical cation, the EPR spectrum depicted as Figure 7b was observed. The hyperfine pattern points to seven protons which are equivalent within the resolution attained. The detection of an even number of lines clearly demonstrates that one ligand must coordinate to Cr(d^5) via benzene and the other via a naphthalene π subsystem [isomer $\mathbf{13}(II)^{+\cdot}$]. If, alternatively, the cocondensate is taken up in methanol and extensively oxidized with air, the spectrum shown in Figure 7c arises. This spectrum is also obtained from analytically pure [**13**][BPh_4]. The well-resolved nonuplet is in accord with the coordination mode of isomer $\mathbf{13}(I)^{+\cdot}$.

The reversible nature of the redox couples **12** (0/−) and **13** (0/−) suggested that intra muros reduction in the cavity of an EPR instrument[25] should yield spectra of the radical anions $\mathbf{12}^{-\cdot}$ and $\mathbf{13}^{-\cdot}$. However, experiments were frustrated by metal−ligand cleavage, possibly at the dianion stage, which could not be avoided due to insufficient control of the potential in the two-electrode set-up. A typical course of events is shown in Figure 6. Upon applying a negative potential to the gold spiral in the electrochemical cell the EPR spectrum due to $\mathbf{12}^{+\cdot}$ (a) becomes gradually superimposed by a new signal, shifted to a g factor which is closer to the free spin value (b). This is in accord with the spectrum expected for the radical anion $\mathbf{12}^{-\cdot}$ since the metal contribution to the LUMO of bis(arene)chromium falls short of that which is contained in the HOMO. Before reaching the stage of reduction where $\mathbf{12}^{-\cdot}$ is the only species present, line broadening sets in which presumably stems from self exchange either of the $\mathbf{12}/\mathbf{12}^{-\cdot}$ or of the $\mathbf{12}^{-\cdot}/\mathbf{12}^{2-}$ type. Alternatively, line broadening could be caused by spin−spin interaction in a biradical dianion $\mathbf{12}^{2-\cdot\cdot}$ generated in the second reduction step. This dianion is very labile, however, since concurrently a signal with $g = 2.0037$ builds up which, upon expansion, is identified as being caused by $\mathbf{9}^{-\cdot}$, the radical anion of the free ligand[26] (c). Unequivocal analysis of the EPR spectrum of $\mathbf{12}^{-\cdot}$ is therefore prevented and the extent of electron delocalization cannot be determined. An analogous situation is encountered in the reduction of **13**; here, as demonstrated by the cyclovoltammetric results, the tendency toward metal−ligand cleavage

Table 4. Crystallographic data for compounds [**12**][BPh_4], [**13**][I]·acetone, and [**13**][I]

Cmpd.	**[12][BPh_4]**	**[13][I]*0.5 acetone**	**[13][I]**
Crystal size [mm]	0.4 x 0.4 x 1	0.3 x 0.3 x 0.1	0.25 x 0.20 x 0.05
Crystal system	monoclinic	orthorhombic	Orthorhombic
Space group	$P2_1/n$, Z= 4	Fdd2 , Z= 16	Pnma , Z= 4
Lattice constants (pm/°]	a = 1537.4(2)	a = 2163.7(1)	a = 2239.2(2)
	b = 1663.6(2) β = 107.1(1)	b = 2697.5(2)	b = 1018.1(1)
	c = 1672.1(4)	c = 1752.1(1)	c = 1044.8(1)
Volume (nm^3)	4.0869(12)	10.2263(11)	2.3818(4)
Formula sum	$C_{60}H_{44}BCr$	$C_{33.5}H_{23}CrIO_{0.5}$	$C_{32}H_{20}CrI$
Formula weight	827.76	612.42	583.38
Density (calc.) (Mg/m^3)	1.345	1.591	1.627
Absorpt. coefficient (mm^{-1})	0.323	1.678	1.795
F(000)	1732	4880	1156
Diffraktometer used	Enraf Nonius CAD4	Stoe IPDS	Stoe IPDS
Wave length	MoKα (71.073 pm)	MoKα (71.073 pm)	MoKα (71.073 pm)
T [K]	193(2)	293(2)	233(2)
Theta range[°]	2.45 to 21.95	2.41 to 25.93	2.15 to 25.90
Index range (h,k,l)	–16/0, 0/17, –16/7	–26/25, –33/33,–20/21	–27/23, –12/12, 12/12
Scan type	Omega	area detector	area detector
Program data collection	CAD4 EXPRESS	Stoe Expose	Stoe Expose
Data reduction	XCAD4 (Harms, 1993)	Stoe Integrate	Stoe Integrate
No. of collected refl.	3703	19778	13447
No. of unique refl.	3575 [R(int) = 0.0228]	4792 [R(int) = 0.0865]	2428 [R(int) = 0.0665]
No. of obs. refl. (>2σ(I))	2572	3550	1460
No. of used reflections	3575	4792	2428
Absorption correction	none	none	Analytical
Max. und min. transmission			0.916, 0.662
Structure solution	direct methods	direct methods	direct methods
Structure refinement	full matrix on F^2	full matrix on F^2	full matrix on F^2
Programs used	SHELXTL–PLUS (Siemens)	SHELXTL–PLUS	SHELXTL–PLUS
	SHELXS–96 (Sheldrick,1996)	SHELXS–96	SHELXS–97 (Sheldruck,1997)
	SHELXL–96 (Sheldrick,1996)	SHELXL–96	SHELXL–97 (Sheldrick, 1997)
Extinction coefficient	0.0010(3)		
Weighting param. q1,q2*	0.0629, 1.0397	0.0595, 0	0.0291, 0
"Goodness–of–fit" on F^2	1.053	0.945	0.833
e–max,min [e/nm^3]	177, –207	558, –360	736, –595
"Flack" parameter		–0.04(3)	
No. of refined parameters	560	327	163
R (observed reflections)	0.0456	0.0405	0.0341
wR2 (used reflections)	0.1166	0.1052	0.0642

* weighting scheme : $w=1/[\sigma^2(Fo^2)+(q1*P)^2+q2*P]$ with $P=(Fo^2+2Fc^2)/3$

of the anion is even more pronounced. As shown in Figure 7d, the EPR spectrum of the free fluoranthene radical anion $\mathbf{10}^{-\cdot}$[27] appears at a stage where the radical cation $\mathbf{13}^{+\cdot}$ is still present in large excess. While $\mathbf{10}^{-\cdot}$ would be expected to be removed instantaneously through electron transfer to $\mathbf{13}^{+\cdot}$, simultaneous observation of both paramagnetic species may be traced to the cell construction[25]. A high local concentration of electrochemical reduction products is generated in a region where EPR sensitivity is maximal, namely near the surface of the gold spiral which serves as the cathode.

We thank the *Deutsche Forschungsgemeinschaft* and the *Fonds der Chemischen Industrie* for support. This work is a part of cooperative project between Ch. E. and A. V. sponsored by the *Volkswagen Stiftung* which we gratefully acknowledge. We are indebted to Prof. *M. Zander* for a gift of triphenylene and for helpful comments.

Experimental Section

General: All manipulations were carried out with exclusion of air under dinitrogen or argon (CV) unless stated otherwise. Physical measurements were performed with the equipment specified previously[28].

Bis[η(1,2,3,4,5,18)triphenylene]chromium (**12**): 5 g (22 mmol) of triphenylene was evaporated from an electrically heated internal

glass vessel held at 10^{-4} Torr within a 6-l glass reactor which was cooled with liquid N_2. Simultaneously, 1.8 g (34.6 mmol) of chromium, contained in a spiral of tungsten wire (∅ 1 mm), was evaporated by a heating current of 40 A at 8 V. The brownish black cocondensate was warmed to room temperature and suspended in 100 ml of toluene. After the access of air, 200 ml of water was added and the red aqueous phase washed with two portions (50 ml) of toluene and one portion of petroleum ether. The aqueous phase was then layered with 150 ml of toluene, exclusion of air provided for and ca. 10 g of $Na_2S_2O_4$ and 10 g of KOH added. Stirring was continued for about 2 h, the aqueous phase then turned colorless and the organic phase brown. Toluene was removed in vacuo and the residue kept at 10^{-4} Torr for 6 h. **12** (280 mg, 1.6% referred to Cr evaporated) was obtained as a dark brown microcrystalline product. Recrystallization was effected by layering a solution of **12** in toluene with petroleum ether (boiling range 40−60°C) and cooling to −20°C. − MS (EI, 70 eV); *m/z* (%): 508 (3.2) [M^+], 280 (4.3) [$M^+ - C_{18}H_{12}$], 228 (100) [$C_{18}H_{12}{}^+$], 52 (10.9) [Cr^+]. − $C_{36}H_{24}Cr$ (508.58): calcd. C 85.04, H 4.72; found C 84.77, H 4.83.

Bis[η(1,2,3,4,5,18)triphenylene]chromium Tetraphenylborate ([**12**][BPh_4]): To the aqueous solution of $\mathbf{12}^{+\cdot}$ obtained from a cocondensation of chromium (1.2 g, 23 mmol) and triphenylene (2 g, 8.7 mmol) performed as described above was added, under stirring, 0.5 g (1.46 mmol) of $NaBPh_4$. The reddish brown precipitate was washed with water and dried in vacuo. − Yield 530 mg (2.8% referred to Cr evaporated). Crystals suitable for X-ray diffraction were obtained by layering of solution of [**12**][BPh_4] (100 mg in 40 ml of acetone) with 120 ml of diethyl ether at 0°C. − $C_{60}H_{44}BCr$ (827.81): calcd. C 87.06, H 5.32; found C 85.67, H 5.41.

Bis[η(1,2,3,4,5,15)fluoranthene]chromium (**13**, isomer I): Chromium (2.1 g, 40.4 mmol) and fluoranthene (8 g, 39.6 mmol) were cocondensed during 2 h at 77 K as described for **12**. The workup procedure followed that given for **12**; in order to generate the radical cation $\mathbf{13}^{+\cdot}$ a stream of air was applied for 1 h before phase separation and reduction. − Yield: 110 mg (0.24 mmol, 0.6% based on Cr evaporated) of **13** as a dark violet microcrystalline product. − ^{1}H- and ^{13}C-NMR: Tables 2 and 3. − MS (EI, 70 eV); *m/z* (%): 456 (2.0) [M^+], 254 (5.1) [$M^+ - C_{16}H_{10}$], 202 (100) [$C_{16}H_{10}{}^+$], 52 (10.0) [Cr^+]. − $C_{32}H_{20}Cr$ (456.51): calcd. C 84.21, H 4.39; found C 84.95, H 5.18.

Bis[η(1,2,3,4,5,15)fluoranthene]chromium Tetraphenylborate ([**13**][BPh_4], isomer I): The reaction mixture from a cocondensation of chromium (1.9 g, 36.5 mmol) and fluoranthene (8 g, 39.6 mmol) was air-oxidized for 1 h. Subsequent manipulations and precipitation of the salt [**13**][BPh_4] followed the instructions given for [**12**][BPh_4]. − Yield: 310 mg (0.40 mmol, 1.1%) of [**13**][BPh_4] as dark red material. Crystals suitable for X-ray diffraction were grown by layering a solution of 140 mg of [**13**][BPh_4] in 60 ml of acetone with 100 ml of diethyl ether at ambient temperature.

Bis[η(1,2,3,4,5,15)fluoranthene]chromium Iodide ([**13**][I], isomer I): Cocondensation of chromium (1.6 g, 30.7 mmol) with fluoranthene (8 g, 39.6 mmol) and subsequent air oxidation (1 h) in the two-phase system H_2O/toluene led to an aqueous solution of $\mathbf{13}^+$ from which dark red [**13**][I] was precipitated by addition of KI (1.0 g, 6.0 mmol). The product was dried in vacuo. − Yield: 470 mg (0.8 mmol, 2.6%). Crystalline material for X-ray diffraction was obtained by layering a solution of 200 mg of [**13**][I] in 80 ml of acetone with 120 ml of diethyl ether. − $C_{32}H_{20}CrI$ (583.41): calcd. C 65.87, H 3.43; found C 66.28, H 3.81.

[η(1′,2′,3′,4′,5′,15′)fluoranthene][η(10,11,12,13,14,16)fluoranthene]chromium (**13**, isomer II): The preparation followed the instructions given for isomer I apart from a shorter (10 min) duration of air oxidation. − Yield 380 mg (0.83 mmol, 2.4%) of a dark violet microcrystalline material. According to ^{1}H NMR, this product was a mixture of ca. 85% of **13**(II) and 15% of **13**(I), see Tables 2 and 3. − $C_{32}H_{20}Cr$ (456.41): calcd. C 84.21, H 4.39; found C 84.87, H 4.93. − The mother liquor of the initial crystallisation was enriched in the more soluble isomer **13**(II). Repeated recrystallisation of the contents of this solution led to a product with the isomer distribution **13**(II)/**13**(I) = 95:5 as gleaned from ^{1}H NMR (see Figure 3 and Tables 2 and 3).

X-ray Crystal Structure Analysis of [**12**][BPh_4] *and* [**13**][I]: The crystal structures were solved by direct methods. Non-hydrogen atoms were refined anisotropically, hydrogen atoms on calculated positions with isotropic temperature factors $U(H) = 1.2\ U_{eq}(C)$. An inspection of the thermal parameters of [**13**][I] indicated unresolved disorder with respect to the crystallographic mirror symmetry. A refinement in the space group $Pna2_1$ (without this mirror symmetry) was not successful. Further details of the crystal structure determinations are given in Table 4.

[1] Ch. Elschenbroich, E. Schmidt, R. Gondrum, B. Metz, O. Burghaus, W. Massa, S. Wocadlo, *Organometallics* **1997**, *16*, 4589.
[2] M. Zander, *Polycyclische Aromaten*, Teubner, Stuttgart, **1995**.
[3] G. Wilkinson, F. G. A. Stone, E. W. Abel, Eds., *Comprehensive Organometallic Chemistry*, Pergamon, Oxford, U.K., **1982**, **1995**.
[4] J. E. Ellis, D. W. Blackburn, P. Yuen, M. Jang, *J. Am. Chem. Soc.* **1993**, *115*, 11616.
[5] [5a] E. P. Kündig, P. L. Timms, *J. Chem. Soc., Chem. Commun.* **1977**, 912. − [5b] Ch. Elschenbroich, R. Möckel, *Angew. Chem. Int. Ed. Engl.* **1977**, *16*, 870; *Angew. Chem.* **1977**, *89*, 908. − [5c] Ch. Elschenbroich, R. Möckel, W. Massa, M. Birkhan, U. Zenneck, *Chem. Ber.* **1982**, *115*, 334.
[6] [6a] E. P. Kündig, C. Perret, S. Spichiger, G. Bernardinelli, *J. Organomet. Chem.* **1985**, *286*, 183. − [6b] N. P. Do Thi, S. Spichiger, P. Paglia, G. Bernardinelli, E. P. Kündig, P. L. Timms, *Helv. Chim. Acta* **1992**, *75*, 2593.
[7] [7a] E. O. Fischer, Ch. Elschenbroich, *J. Organomet. Chem.* **1967**, *7*, 481. − [7b] Evidence for the possible existence of $(\eta^6\text{-}C_{10}H_8)_2Fe$ has been derived from matrix isolation studies: P. D. Morand, C. G. Francis, *Organometallics* **1985**, *4*, 1653.
[8] Ch. Elschenbroich, E. Bilger, R. Möckel, *Z. Naturforsch., B* **1983**, *38*, 1357.
[9] Ch. Elschenbroich, R. Möckel, *Z. Naturforsch., B* **1984**, *39*, 375.
[10] Ch. Elschenbroich, J. Schneider, W. Massa, G. Baum, H. Mellinghoff, *J. Organomet. Chem.* **1988**, *355*, 163.
[11] M. Jang, J. E. Ellis, *Angew. Chem. Int. Ed. Engl.* **1994**, *33*, 1973; *Angew. Chem.* **1994**, *106*, 2036.
[12] M. K. Pomije, C. J. Kurth, J. E. Ellis, M. V. Barybin, *Organometallics* **1997**, *16*, 3582.
[13] Ch. Elschenbroich, J. Heck, F. Stohler, E. Bilger, *Chem. Ber.* **1984**, *117*, 23.
[14] M. Randic, *Tetrahedron* **1975**, *31*, 1477.
[15] R. D. Rodgers, J. L. Atwood, T. A. Albright, W. A. Lee, M. D. Rausch, *Organometallics* **1984**, *3*, 263.
[16] B. Deubzer, E. O. Fischer, H. P. Fritz, C. G. Kreiter, N. Kriebitzsch, H. D. Simmons, Jr., B. R. Willeford, Jr., *Chem. Ber.* **1967**, *100*, 3084.
[17] Apart from the torsional angle, the structural parameters of [**13**][I]·0.5 acetone differ insignificantly from those of the solvent-free sample. The crystal quality of [**13**][BPh_4] was insufficient for refinement.
[18] F. R. Ahmed, J. Trotter, *Acta Crystallogr.* **1963**, *16*, 503.
[19] A. C. Hazell, D. W. Jones, J. M. Sowden, *Acta Crystallogr.* **1977**, *B33*, 1516.
[20] F. G. N. Cloke, A. R. Dias, A. M. Galvão, J. L. Ferreira da Silva, *J. Organomet. Chem.* **1997**, *548*, 177.
[21] [21a] Ch. Elschenbroich, E. Bilger, B. Metz, *Organometallics*

1991, *10*, 2823 for further references. – [21b] H. Binder, Ch. Elschenbroich, *Angew. Chem. Int. Ed. Engl.* **1973**, *12*, 659; *Angew. Chem.* **1973**, *85*, 665.
[22] $E_{1/2}(\text{triphenylene}^{0/-}) = -2.49$ V; $E_{1/2}(\text{fluoranthene}^{0/-}) = -1.77$ V: A. Streitwieser, *Molecular Orbital Theory for Organic Chemists*, Wiley, New York, **1961**, p. 178.
[23] Ch. Elschenbroich, J. Koch, J. Schneider, B. Spangenberg, *J. Organomet. Chem.* **1986**, *317*, 41; Ch. Elschenbroich, R. Möckel, U. Zenneck, D. W. Clack, *Ber. Bunsenges. Phys. Chem.* **1979**, *83*, 1008 and papers cited therein.
[24] Ch. Elschenbroich, F. Gerson, *J. Organomet. Chem.* **1973**, *49*, 445.
[25] R. D. Allendoerfer, G. A. Martinchek and S. Bruckenstein, *Anal. Chem.* **1975**, *47*, 890.
[26] M. T. Jones, R. H. Ahmed, *J. Phys. Chem.* **1980**, *84*, 2913.
[27] F. Gerson, *Hochaufgelöste ESR-Spektroskopie*, VCH, Weinheim, **1967**, p. 108.
[28] Ch. Elschenbroich, P. Kühlkamp, A. Behrendt, K. Harms, *Chem. Ber.* **1996**, *129*, 859.

[98055]